https://doi.org/10.5194/egusphere-2024-2940
Preprint. Discussion started: 15 October 2024

Investigating Plant Responses to Water Stress via Plant Hydraulics Pathway

Zengjing Song[1,2], Yijian Zeng[2], Yunfei Wang[2,3], Enting Tang[2], Danyang Yu[2], Fakhereh (Sarah) Alidoost[4], Mingguo Ma[1], Xujun Han[1], Xuguang Tang[5], Zhongjing Zhu[1], Yao Xiao[1], Debing Kong[1], Zhongbo (Bob) Su[2]

[1]School of Geographical Sciences, Southwest University, Chongqing, 400715, China
[2]Faculty of Geo-Information Science and Earth observation (ITC), University of Twente, Enschede, 7500 AE, the Netherlands
[3]School of Water Conservancy and Transportation, Zhengzhou University, Zhengzhou, 45001, China
[4]Netherlands eScience Center, Amsterdam, 1098XH, the Netherlands
[5]Institute of Remote Sensing and Geosciences, Hangzhou Normal University, Hangzhou, 311121, China

Correspondence to: Zhongbo (Bob) Su (z.su@utwente.nl); Yijian Zeng (y.zeng@utwente.nl); Xujun Han (hanxujun@swu.edu.cn)

Abstract. Drought-induced plant hydraulic failure is one of the main factors for large-scale plant mortality. Understanding the response of the plants to water stress is of paramount importance to elucidate the dynamics of water, energy and carbon fluxes under drought conditions. In this study, we implemented the plant hydraulics pathway in STEMMUS-SCOPE (hereafter as STEMMUS-SCOPE-PHS) by considering xylem vulnerability, and validated the model at a karst site in Chongqing, China. Plant water potentials of root, stem and leaf are calculated in STEMMUS-SCOPE-PHS. A leaf water potential-based plant water stress factor (PHWSF) replaces the original soil moisture-based water stress factor to represent the effect of water stress on plant growth. Results show that the PHWSF captures the diurnal dynamics of water stress. The STEMMUS-SCOPE-PHS improves the simulation of diurnal dynamics of latent heat flux, net ecosystem exchange and gross primary production compared to STEMMUS-SCOPE with the value of Kling-Gupta efficiency (KGE) increasing from 0.74 to 0.83, 0.57 to 0.76, and 0.57 to 0.80, respectively. This research delineates the plant hydraulic responses to water stress and highlights the importance of leaf water potential in reflecting the plant water stress.

1 Introduction

Plant hydraulics describes water transport within plant vessel systems, involving root water uptake, sap flow, and transpiration, directly impacting crop yield and food security (Torres-Ruiz et al., 2024). Drought-induced plant hydraulic failure is one of the dominant reasons for large-scale plant mortality (Mcdowell et al., 2019; Adams et al., 2017; Anderegg et al., 2015; Anderegg et al., 2016; Choat et al., 2018), which reduces the gross primary productivity (GPP), potentially transforms an ecosystem from carbon sink to carbon source (Gatti et al., 2021), and alters the evapotranspiration and precipitation feedback at regional scale (Limousin et al., 2009). A comprehensive understanding of plant hydraulics is a vital prerequisite for exploring

https://doi.org/10.5194/egusphere-2024-2940
Preprint. Discussion started: 15 October 2024

the response of plants to drought, improving the prediction of tree mortality (Anderegg et al., 2015) and enhancing the protection of biodiversity (Anderegg et al., 2018).

Water stress is utilized to quantify the effects of droughts, from both soil and atmosphere, on plant physiological and biochemical processes (Torres-Ruiz et al., 2024), such as stomata opening and photosynthesis. Water stress can be characterized well by in-situ observations of soil moisture, plant water content, and leaf water potential, yet, such observations are limited to point scale with the scarcity of available data. Microwave-based remote sensing data enables the evaluation of global water stress conditions via vegetation optical depth (Konings and Gentine, 2017), but it remains a challenge to derive process-relevant long time-series and high-resolution spatiotemporal information (e.g. sub-daily dynamics of water potential at the tree-level). Physics-based Earth System Models (ESMs) (Lawrence et al., 2019; Li et al., 2021; Tyree and Ewers, 1991) enable to simulate and predict water stress at various spatiotemporal scales, ranging from minutes to decades, and from sites to ecosystem scale, overcoming the limitation of in-situ and remote sensing observations.

STEMMUS-SCOPE is a Soil-Plant-Atmosphere Continuum (SPAC) model integrating the processes of soil water and heat transfer, canopy radiation transfer, energy balance and photosynthesis (Wang et al., 2021). It has been evaluated over 172 flux tower sites (Abramowitz et al., 2024; Wang et al., 2021; Tang et al., 2024; Wang et al., 2024) across the world covering 11 land covers. The results showed that the STEMMUS-SCOPE systematically underestimated the Bowen ratio ($\frac{H}{LE}$, where H is sensible heat flux, and LE is latent heat flux) across 170 flux tower sites, indicating more energy was allocated to latent heat flux for transpiration, accompanied by an underestimation of water use efficiency ($\frac{NEE}{LE}$, where NEE is net ecosystem exchange) for the same NEE (Abramowitz et al., 2024). The low water use efficiency indicated a generous water-use strategies, and potentially suggested an underestimation on water stress.

In STEMMUS-SCOPE (version 1.0.0), the water stress factor has a range from 0 - 1 (the smaller the value, the greater the water stress), which is based on root zone soil moisture, root length distribution and soil hydraulic properties that are determined by soil water balance, dynamic root growth, and soil texture (Wang et al., 2021). However, it does not consider the water stress induced by either interior plant hydraulics or from the atmosphere evaporative demand (Xu et al., 2016; Li et al., 2021; Xie et al., 2023). Therefore, the soil moisture (or soil water potential) based water stress factor (SMWSF) is limited in explicitly describing plant's responses to water stress, and can introduce uncertainties in the simulation of carbon, water and energy fluxes (Powell et al., 2013; Tuzet et al., 2003). In fact, the water transport within the plant vessel system can be described by Darcy's Law ($q = K \times \frac{\Delta h}{L}$, where q is water flux, K is hydraulic conductivity, Δh is the water potential gradient, and L is the distance over water potential drops). A large water potential gradient stimulates a larger water flux in the xylem, resulting in a larger tension that may facilitate embolism formation, which in turn decreases the hydraulic conductivity and increases the xylem vulnerability. In STEMMUS-SCOPE, the above plant hydraulic process is simplified as a series of hydraulic resistances (Wang et al., 2021).

Leaf water potential hydraulically links the water states of soil, plant and atmosphere (Zeng and Su, 2024), and is recognized as an indicator of plant water status in recent developments of land surface models (LSMs) (Kennedy et al., 2019; Li et al.,

https://doi.org/10.5194/egusphere-2024-2940
Preprint. Discussion started: 15 October 2024

2021; Xu et al., 2016; Xie et al., 2023). Coupling plant hydraulics pathway in LSMs enables the determination of plant water potentials (root, stem and leaf), to accurately reflect water stress, to capture responses of different plant species on water stress under similar weather conditions, and to improve the estimation of water, energy and carbon fluxes (Xu et al., 2016; Kennedy et al., 2019; Li et al., 2021; Xie et al., 2023; Mackay et al., 2015; Anderegg et al., 2018). For example, Community Land Model Version 5.0 (CLM5) introduced leaf water potential-based water stress factor (PHWSF) to explore the sensitivity of vegetation to drought at a tropical evergreen forest in Brazil, under both ambient precipitation conditions and 60% of precipitation-throughfall-exclusion conditions. Results showed that CLM5 is more sensitive to atmospheric drought than CLM4.5, which uses an SMSWF (Kennedy et al., 2019). Xu et al. (2016) coupled plant hydraulics into the ED2 model and defined new plant function types based on plant hydraulic traits, enabling the model to capture diverse phenology for different plant species in seasonally dry tropical forests. Li et al. (2021) proposed the big-tree conception by considering whole plant hydraulics with water storage in the Noah-MP model (i.e. Noah-MP-PHS), and the results showed that Noah-MP-PHS captured different hydraulics behaviours of isohydric (red-maple) and an-isohydric (red-oak) during a dry-down period in Michigan, USA. Xie et al. (2023) improved the Vegetation Interface Process model (VIP) with plant hydraulics (VIP-PHS) and validated VIP-PHS in 30 FLUXNET sites. Results showed VIP-PHS reduced 44% of RMSE for evapotranspiration and more than 50% of RMSE for gross primary productivity (GPP) compared with the original VIP model.

Previous studies validated plant hydraulics in dry regions or seasonal-drought regions with both low precipitation and low soil moisture. Karst regions in Southwest China are characterized by high annual precipitation, but plants are always suffering from drought because of the thin soil layer and strong drainage due to rock cracks (Song et al., 2019). Can we improve our knowledge of the response of plants to drought over the karst region by considering plant hydraulics in the STEMMUS-SCOPE model? To answer this research question, we integrated an explicit plant hydraulic module into the STEMMUS-SCOPEv1.0.0 (hereafter STEMMUS-SCOPE-PHS), by considering the xylem vulnerability, plant water potential (of root, stem and leaf) and plant water stress. The STEMMUS-SCOPE-PHS is evaluated at a karst site (Hutoucun site) in southwest China from 1st January to 9th August, 2022. The simulation of water, energy and carbon fluxes, as well as stem water potential, are validated against in-situ observations. The objectives of this study are (a) to couple the plant hydraulics module into STEMMUS-SCOPE model, (b) to investigate the performance of plant hydraulic model at a karst ecosystem, (c) to answer how plants respond to drought from a perspective of plant hydraulics. The structure of the study is organized as follows: Section 2 introduces the research area and dataset, as well as the framework of the plant hydraulics pathway in the STEMMUS-SCOPE-PHS. Section 3 reports the model performance in simulating water, energy and carbon fluxes. The effects of plant hydraulics on terrestrial carbon and water cycling are discussed in Section 4. Section 5 summarizes the main conclusions of this study.

https://doi.org/10.5194/egusphere-2024-2940
Preprint. Discussion started: 15 October 2024

2 Methodology

2.1 Study area

The Hutoucun site (HTC, 106.3192° E, 29.7627° N, 473 m a.s.l.) is located in a well-developed karst region in southwest of Chongqing, China (Fig. 1). This area characterizes a subtropical monsoon climate, and the weather is moderate and rainy. The annual average temperature is 15-17 °C, and the mean air temperature of the coldest month (January) and warmest month (August) are about 2 °C and 40 °C, respectively. The annual precipitation is about 1240 mm (Xiao et al., 2021) with the most occurring from April to July. The large amount of precipitation causes the high relative humidity, and cloudy and foggy climate. The karst topography is characterized by a thin soil layer on the surface and lots of rock cracks in the bedrock, which makes it easier for precipitation to infiltrate and form underground rivers rather than being stored in the soil (Song et al., 2019). Plants always experience water stress during a relatively dry period despite abundant annual precipitation.

2.2 Data

The data is collected from a flux tower (10 m) over an *Osmanthus fragrans* plantation, with an average tree height of 3-3.5 m. An automatic weather station (AWS) and an eddy-covariance (EC) measurement system were installed on the flux tower at the end of 2018. The AWS collects data including air temperature (T_{air}), relative humidity (RH), wind speed (U), precipitation ($Precip$), upward/downward longwave ($LWup$, $LWdown$) and shortwave ($SWup$, $SWdown$) radiations. Photosynthetically active radiation (PAR) is observed below (3 m) and above (10 m) the canopy, respectively. An open-path EC system (LI-COR 7500, USA) was installed to measure the water and carbon fluxes at the height of 5 m. The raw EC data (10 Hz) were first averaged into half-hourly data with the EddyPro software (LI-COR, USA). The net ecosystem exchange (NEE) was then split into the gross primary production (GPP) and the ecosystem respiration (Re) with an R package: REddyproc (https://www.bgc-jena.mpg.de/5624551/REddyProc-Rpackage, Max Planck Institute, last accessed on 28th July, 2024) (Wutzler et al., 2018). An automatic solar-induced chlorophyll fluorescence (SIF) system was conducted since 2021, detailed information can be found in Wang et al. (2023).

The soil texture is sandy loam and silt loam at the surface and deep layers, respectively. Soil moisture and soil temperature probes were installed at the depth of 5, 10, 20, 40, 60, and 80 cm. Three soil heat flux plates were placed horizontally in parallel at the depth of 5 cm. A set of PSY-1 Plant Stem Psychrometer was installed in a branch to collect in-situ xylem water potential from 27th July to 20th September, 2022. The leaf area index (LAI) was collected from MODIS MCD15A2H.006, an 8-day composite LAI dataset with a spatial resolution of 500 m via Google Earth Engine. Quality control flags were used to remove pixels affected by clouds. The quality-controlled LAI data was interpolated into half-hourly temporal resolution, and calibrated with 5-day (5th July, 14th July, 1st September, 6th September, and 2nd October) in-situ observed LAI, and then filtered further by the Harmonic Analysis of Time Series (HANTS) method (Supplement Fig. S1) in Matlab 2021a (Mathworks, the USA).

https://doi.org/10.5194/egusphere-2024-2940
Preprint. Discussion started: 15 October 2024

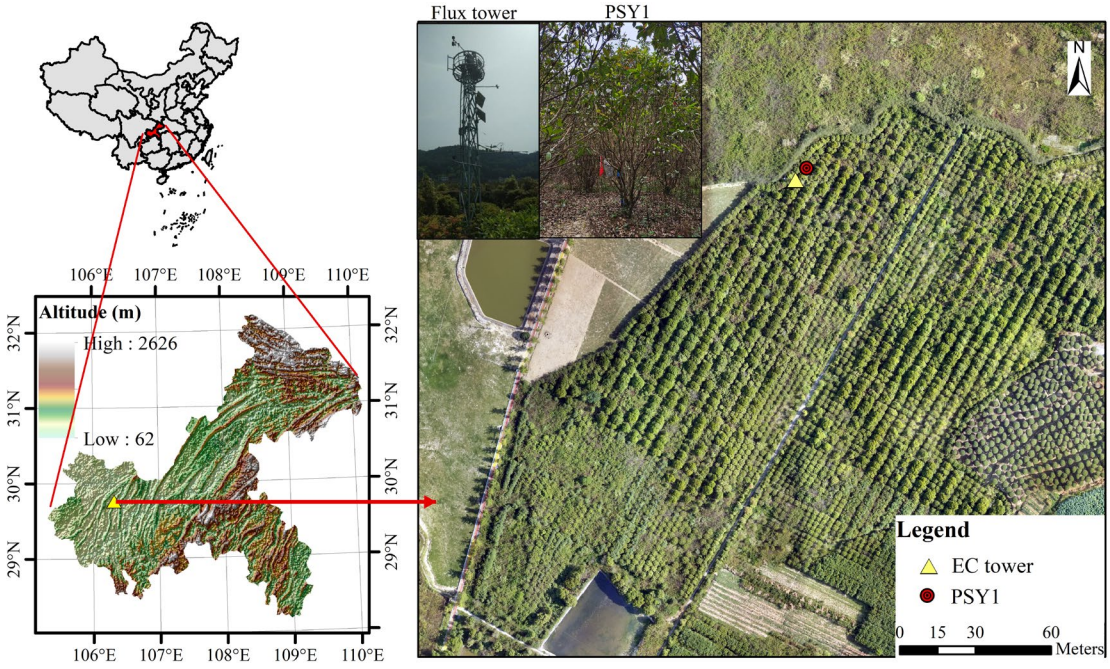

Figure 1: Study area. In this figure, the 1-km resolution Digital Elevation Model (DEM) was downloaded from the Resource and Environmental Science Data Platform (https://www.resdc.cn/data.aspx?DATAID=123, last accessed on 28th, July 2024), and the high-resolution optical image was obtained by DJI Phantom 4 on August 10th, 2022.

2.3 STEMMUS-SCOPE

The STEMMUS-SCOPE model is an elaborate process-based model which integrates simultaneous energy, mass and momentum transport in soil and plant, and also the radiation transfer, and biochemical process in the canopy (Wang et al., 2021; Van Der Tol et al., 2009; Zeng et al., 2011a, b; Tang et al., 2024). It consists of the Simultaneous Transfer of Energy, Mass and Momentum in Unsaturated Soil (STEMMUS) model (Zeng et al., 2011b, a) and the Soil Canopy Observation of Photochemistry and Energy fluxes (SCOPE) model (Van Der Tol et al., 2009). In STEMMMUS-SCOPE, water and heat fluxes in SPAC are fully coupled, and the model also accounts for the transport of vapor and dry air in unsaturated soil is considered. Additionally, it is capable of simulating multiple layers of spectra information and SIF, making it possible to compare with in-situ and satellite SIF data. Therefore, it's a terrific tool to explore the interactions and feedback between land and atmosphere in terrestrial ecosystems.

In STEMMUS-SCOPE, the stomatal conductance is calculated based on Ball et al. (1987), in which the stomatal conductance is regulated by relative humidity, carbon dioxide concentration and carbon assimilation amount (See Appendix A1). It empirically assumed that the stomatal conductance is determined by relative humidity but ignored the dependence on peri-stomatal water flux (Medlyn et al., 2011). Secondly, the soil moisture-based water stress factor at the ith soil layer (SMWSF(i)) was calculated as a sigmoid function ($SMWSF(i) = \frac{1}{1+e^{-100\theta_{sat}\left(SM(i)-\frac{\theta_f+\theta_w}{2}\right)}}$, where θ_i is soil moisture at ith layer, θ_{sat} is soil

https://doi.org/10.5194/egusphere-2024-2940
Preprint. Discussion started: 15 October 2024

saturated soil moisture, θ_w is permanent wilting point and θ_f is field capacity). The multiple-layer water stress factors are integrated into a single value that represents soil water stress in the root zone, weighted by the ratio of root length (Wang et al., 2021). The calculation of SMWSF ignores the impacts of plant water status, such as leaf water potential and atmospheric evaporative demand (increasing vapour pressure deficit), on photosynthesis. Furthermore, the resistances of water flow from soil to leaves were divided into three parts: the soil hydraulic resistance, root radial resistance, and plant axial resistance, which were simplified as a function of root length density. It ignored the mechanism of xylem vulnerability, simplifying the water transport in the plant vessel system. To overcome the above drawbacks, this study aims to couple the plant hydraulics (PHS) process into the STEMMUS-SCOPE model (hereafter STEMMUS-SCOPE-PHS) to explore the plant response to water stress via plant hydraulics and to enhance its representation of biophysical and mechanistic processes in a forest ecosystem.

2.4 STEMMUS-SCOPE-PHS

2.4.1 Stomatal conductance scheme

In STEMMUS-SCOPE-PHS, a semi-empirical optimal stomatal conductance model (Medlyn et al., 2011) is employed to represent the potential influence of the increasing vapour pressure deficit on stomatal regulation,

$$g_s = g_0 + 1.6 \cdot \left(1 + \frac{g_1}{\sqrt{D}}\right)\left(\frac{A_n}{c_a}\right), \quad (1)$$

where g_s is stomatal conductance ($\mu mol\, m^{-2}s^{-1}$) for water molecule, g_0 is the minimal stomatal conductance ($\mu mol\, m^{-2}s^{-1}$), g_1 is the slope of stomatal conductance ($kPa^{0.5}$), D is water vapor pressure deficit (kPa), A_n is the net carbon assimilation rate ($\mu mol\, m^{-2}s^{-1}$), C_a is the CO_2 concentration at the leaf surface ($\mu mol\, mol^{-1}$). 1.6 is the scale factor for converting conductance of CO_2 to that of water vapor.

2.4.2 Water fluxes in plant hydraulics

The plant hydraulics pathway describes the process from water absorbed by roots to water released through stomata (Fig. 2). The STEMMUS-SCOPE-PHS assumes that the water demand by the plant equals the water supply by the soil, while assuming the water storage in the plant is constant.

$$\sum_{i=1}^{n} q_{soil-root,i} = q_{root-stem} = q_{stem-leaf} = q_{leaf-air} = Trans, \quad (2)$$

where the $q_{soil-root,i}, q_{root-stem}, q_{stem-leaf}, q_{leaf-air}$ represent the water fluxes (m s^{-1}) from soil to roots, roots to stem, stem to leaf, and leaf to air, respectively. The $Trans$ means transpiration (m s^{-1}). The subscript *i* indicates the i^{th} soil layer. The plant tissues are assumed to be a porous medium. Therefore, the water fluxes can be described based on Darcy's law:

$$q_{soil,i-root,i} = k_{soil-root,i} \times \left(\psi_{soil,i} - \psi_{root,i} - z_i\right), \quad (3)$$

https://doi.org/10.5194/egusphere-2024-2940
Preprint. Discussion started: 15 October 2024

where $k_{soil-root,i}$ (s^{-1}) means the hydraulic conductance from soil to root in the i^{th} soil layer. $\psi_{soil,i}$ (m) means soil water potential in i^{th} soil layer. $\psi_{root,i}$ means root water potential in the i^{th} soil layer. z_i (m) means the depth of i^{th} soil layer.

$$q_{root-stem} = k_{root-stem} \times SAI \times (\psi_{root} - \psi_{stem} - h), \quad (4)$$

where $k_{root-stem}$ (s^{-1}) is hydraulic conductance from root to stem. SAI ($m^2 m^{-2}$) is stem area index, ψ_{root} (m) is the average root water potential at the soil surface. ψ_{stem} (m) is stem water potential. h (m) is the height of the canopy that is equal to gravitational potential.

$$q_{stem-leaf} = k_{stem-leaf} \times LAI \times (\psi_{stem} - \psi_{leaf}), \quad (5)$$

where $k_{stem-leaf}$ (s^{-1}) is hydraulic conductance from stem to leaf. LAI ($m^2\ m^{-2}$) is leaf area index, ψ_{leaf} (m) is leaf water potential.

The transpiration can be calculated based on energy balance model.

$$Trans = \frac{LE}{\lambda}, \quad (6)$$

where LE (W m^{-2}) is latent heat flux, λ (J mol^{-1}) is latent heat of vaporization.

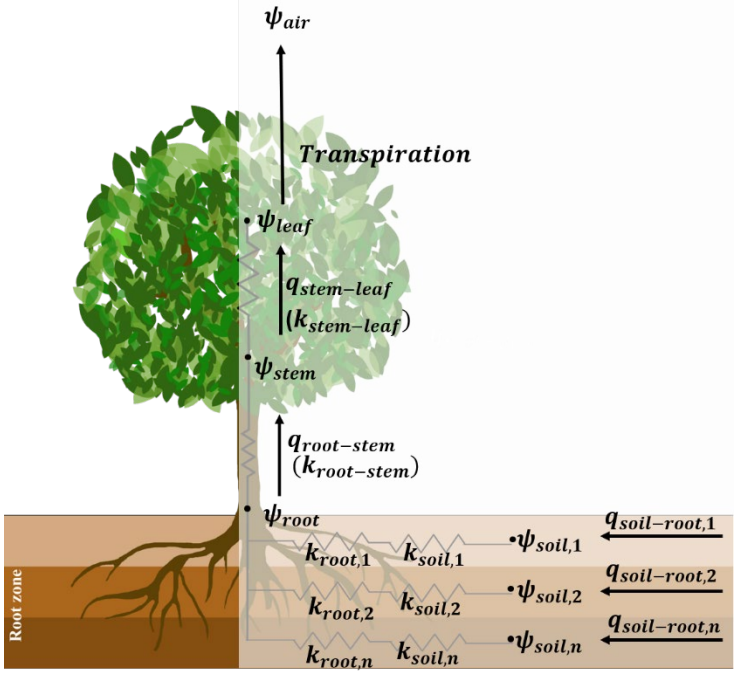

Figure 2: Sketch of plant hydraulics pathway in STEMMUS-SCOPE-PHS.

https://doi.org/10.5194/egusphere-2024-2940
Preprint. Discussion started: 15 October 2024

2.4.3 Plant water stress factor

In STEMMUS-SCOPE, the stomatal conductance, transpiration and carbon assimilation are fully coupled based on the Farquhar et al. (1980) model. The water stress effect on photosynthesis is represented by multiplying water stress factor by the maximum carboxylation rate under a well-watered condition ($Vcmax$, $\mu mol\ m^{-2}s^{-1}$) (Kennedy et al., 2019).

$$Vc = Vcmax \times phwsf \tag{7}$$

where Vc ($\mu mol\ m^{-2}s^{-1}$) is the carboxylation rate considering the water stress effect on photosynthesis.

Two parameterizations of water stress factor were coupled into the STEMMUS-SCOPE-PHS to account for different types of plants. The plant water stress factor $phwsf_{ED2}$ (Xu et al., 2016) is set as the default option in the STEMMUS-SCOPE-PHS. It can be calculated as

$$phwsf_{ED2} = \left[1 + \left(\frac{\psi_{leaf}}{P50_{leaf}}\right)^{a}\right]^{-1}, \tag{8}$$

where $P50_{leaf}$ (m) is the water potential at the 50% hydraulic conductance loss and a is a shape parameter.

The other optional parameterization of plant water stress factor $phwsf_{CLM}$ (Kennedy et al., 2019) is calculated as

$$\mathrm{phws}f_{CLM} = 2^{-\left(\frac{\psi_{leaf}}{P50_{leaf}}\right)^{ck_{leaf}}}, \tag{9}$$

where ck_{leaf} is a shape factor.

All the related functions are listed in Appendix. The values of parameters are listed in Supplement S3.

2.5 Performance evaluation metrics

The simulation performance is evaluated with the coefficient of determination (R^2), mean bias error (MBE), root mean square error (RMSE) and Kling-Gupta efficiency (KGE)

$$R^2 = 1 - \frac{\sum_{i=1}^{n}(\mathrm{obs_i} - \mathrm{sim_i})^2}{\sum_{i=1}^{n}\left(\mathrm{obs_i} - \overline{obs}\right)^2}, \tag{10}$$

$$MBE = \frac{1}{n}\sum_{i=1}^{n}(sim_i - obs_i) \tag{11}$$

$$RMSE = \sqrt{\frac{1}{n}\sum_{i=1}^{n}(sim_i - obs_i)^2}, \tag{12}$$

https://doi.org/10.5194/egusphere-2024-2940
Preprint. Discussion started: 15 October 2024

$$\mathrm{KGE} = 1 - \sqrt{(r-1)^2 + \left(\frac{\sigma_{sim}}{\sigma_{obs}} - 1\right)^2 + \left(\frac{\overline{sim}}{\overline{obs}} - 1\right)^2}, \quad (13)$$

where sim_i is value of the i[th] simulation, and obs_i is value of the i[th] observation. $\overline{sim}$ and $\overline{obs}$ are the average values of the simulation and observation, respectively. The i means the number of time steps, n is the total number of time steps during the study period. The r is the Pearson correlation coefficient, σ_{sim} and σ_{obs} are standard deviations of simulation and observation data, respectively. It should be noted that the value of KGE closer to 1 means the better performance of models.

3 Results

3.1 STEMMUS-SCOPE-PHS vs STEMMUS-SCOPE

The simulated and observed half-hourly energy fluxes are compared in Fig. 3. Generally, the results show that the STEMMUS-SCOPE-PHS model has a better performance than the original STEMMUS-SOCPE with a higher value of KGE. Both models show good agreement for the simulation of net radiation (Rn) with an R^2 value of 0.99, and an MBE (RMSE) value of -12.10 (31.12) W m^{-2} for STEMMUS-SCOPE and -10.50 (28.62) W m^{-2} for STEMMUS-SCOPE-PHS. The KGE values for STEMMUS-SCOPE and STEMMUS-SCOPE-PHS are 0.81 and 0.84, respectively. The STEMMUS-SCOPE-PHS shows better performance for the simulation of latent heat flux (LE) than STEMMUS-SCOPE with a higher value of R^2 (0.69 vs 0.66), slightly lower value of RMSE (39.46 vs 40.96 W m^{-2}) and the closer to 1 value of KGE (0.83 vs 0.74). For the sensible heat flux (H), statistic proxies (R^2 and RMSE) show that the result of STEMMUS-SCOPE-PHS is approximately equal to that of STEMMUS-SCOPE, although the values of KGE show that the performance of STEMMUS-SCOPE-PHS (0.70) is better than that of the STEMMUS-SCOPE (0.52). The two models overestimate soil heat flux (G) in the nighttime ($G < 0$) and underestimate G in the daytime ($G > 0$) with the value of R^2, MBE, RMSE, and KGE for STEMMUS-SCOPE-PHS versus STEMMUS-SCOPE are 0.39 vs. 0.39, 0.51 vs 0.57 W m^{-2}, 25.49 vs. 25.87 W m^{-2} and 0.57 vs. 0.56, respectively. The reason will be further discussed in Section 4.1.

https://doi.org/10.5194/egusphere-2024-2940
Preprint. Discussion started: 15 October 2024

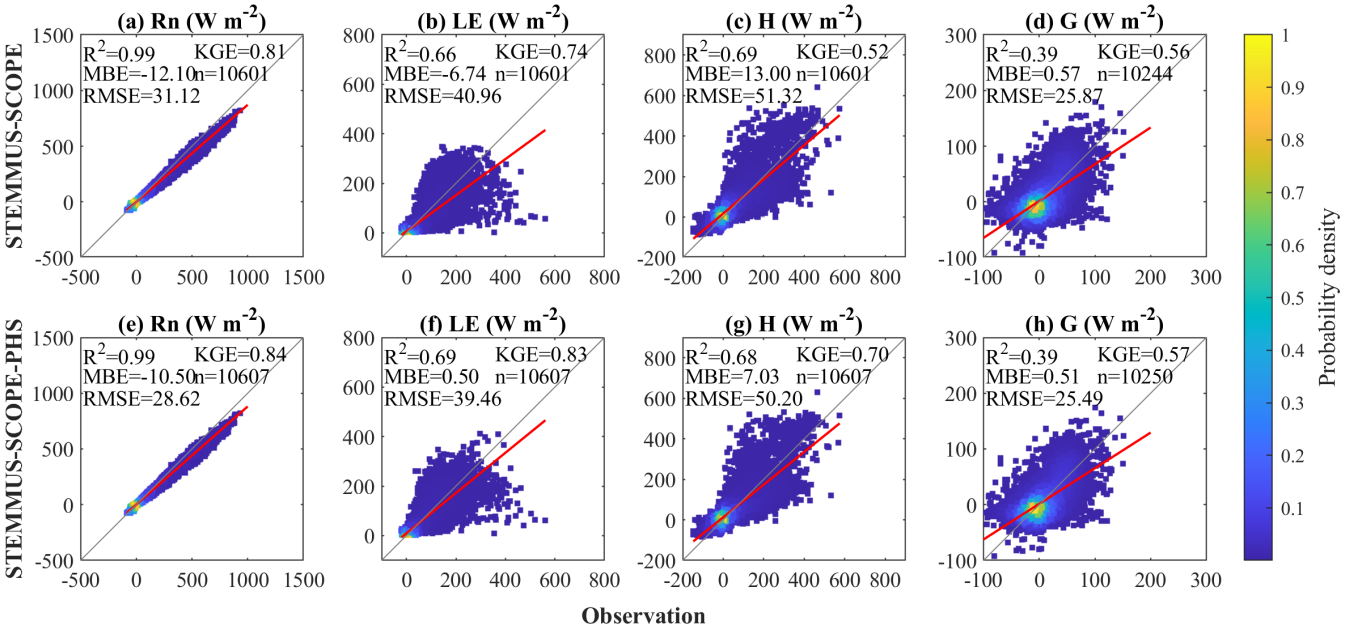

Figure 3: Comparison of half-hourly simulated and observed net radiation (Rn) (a & e), latent heat flux (LE) (b & f), sensible heat flux (H) (c & g), and soil heat flux (G) (d & b) based on STEMMUS-SCOPE (a-d) and STEMMUS-SCOPE-PHS (e-f) at Hutoucun site. The x-axis represents observation, and the y-axis represents simulation. The grey line is 1:1 line, and the bold red line is the regression line. The values of R^2, MBE, RMSE, KGE and the numbers of points (n) are given in each subplot.

Comparison of half-hourly net ecosystem exchange (NEE), gross primary productivity (GPP), SIF, and photosynthetic active radiation (PAR) are shown in Fig. 4. Statistically, the PHS model improves the simulation of NEE (GPP), increasing the R^2 from 0.78 (0.79) to 0.82 (0.82) and reducing the RMSE from 3.97 (4.11) to 2.79 (2.97) $\mu molm^{-2}s^{-1}$, and has better performance for simulated carbon fluxes with values of KGE increase from 0.57 (0.57) by STEMMUS-SCOPE to 0.76 (0.80) by STEMMUS-SCOPE-PHS for NEE (GPP). Furthermore, the overestimation of NEE and GPP are improved as shown in Fig. 4 (a & e, b & f). Both models correctly simulate PAR but overestimate SIF compared with observation. Although the improvement of SIF is beyond the aim of this research, the potential reasons for the deviations in simulating SIF will be further discussed in Section 4.2.

https://doi.org/10.5194/egusphere-2024-2940
Preprint. Discussion started: 15 October 2024

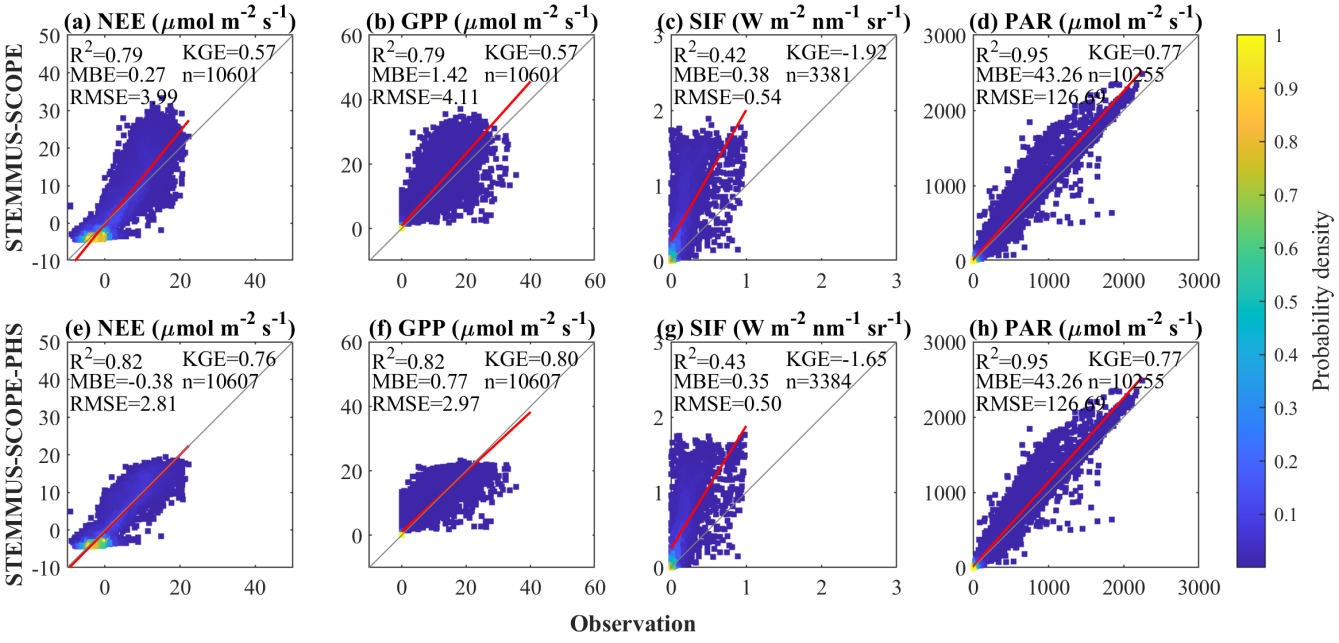

Figure 4: Comparison of half-hourly simulated and observed net ecosystem exchange (NEE), (a & e), gross primary productivity (GPP) (b & f), solar-induced chlorophyll fluorescence (SIF) (c &g), and photosynthetically active radiation (PAR) (d & h) based on STEMMUS-SCOPE (a-d) and STEMMUS-SCOPE-PHS (e-h) at Hutoucun site. The x-axis represents observation, and the y-axis represents simulation. The grey line is the 1:1 line. The bold red line is the regression line. The values of R^2, MBE, RMSE, KGE, and the numbers of points (n) are given in each subplot.

3.2 Improved dynamics in land fluxes via coupling plant hydraulics

The time-series dynamics of energy and carbon fluxes with different water stress factor schemes are shown in Supplement Fig. S4 and Supplement Fig. S5. In general, the plant hydraulics water stress factor (PHWSF) in STEMMUS-SCOPE-PHS shows clearly diurnal dynamics compared with the SMWSF in STEMMUS-SCOPE. Two sub-periods are selected to further evaluate the model performance under different soil water stress conditions according to SMWSF. As shown in Fig. 5, the SMWSF is approximately equal to 1 from DOY 110-117, which indicates a water-well condition. For DOY 208-215 (Fig. 6), the SMWSF is 0.6-0.8, which indicates a water-limited condition.

Under water-well conditions (Fig. 5(a)) and water-limited conditions (Fig. 6(a)), the PHWSF represents the plant water stress that varies with transpiration on a sub-daily scale. The PHWSF shows higher values in the morning and evening (i.e., little water stress) but lower values in the afternoon (i.e., more water stress). This is because the transpiration increases in the afternoon, leading to higher water consumption, resulting in greater water stress. The water stress is relieved in the evening due to a decrease in water demand with a lower temperature and a decreased downward shortwave radiation.

Overall, the SMWSF overestimates the water stress factor in the afternoon and overestimates the latent heat flux (Fig. 5(b) and Fig. 6(b)) and CO_2 assimilation (Fig. 5(d) and Fig. 6(d)). The PHWSF factor captures the diurnal cycles of water stress and improves the simulation of latent heat flux and GPP.

https://doi.org/10.5194/egusphere-2024-2940
Preprint. Discussion started: 15 October 2024

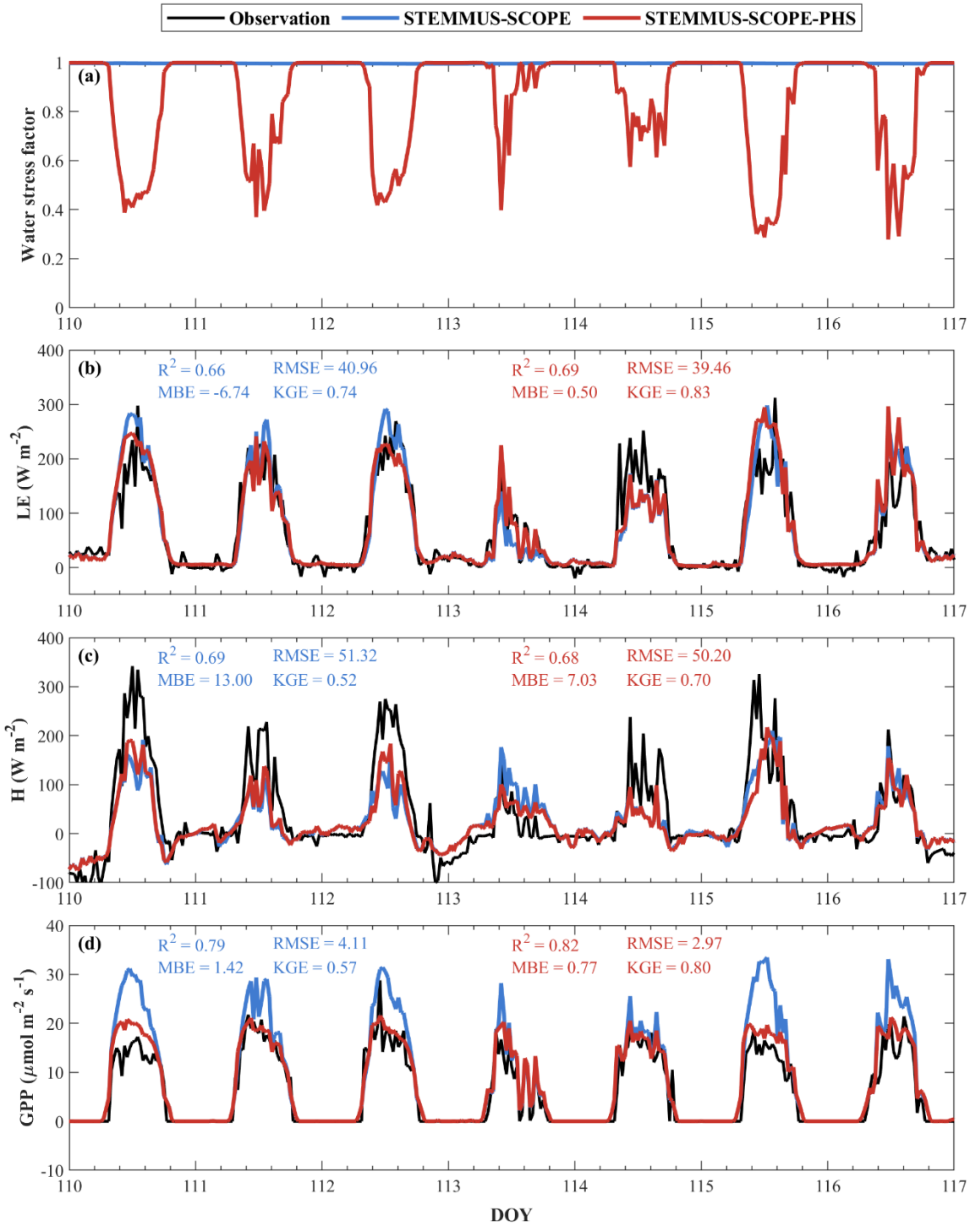

Figure 5: Diurnal dynamics for (a) water stress factor, (b) latent heat flux (LE, W m^{-2}), (c) sensible heat flux (H, W m^{-2}), and (d) gross primary productivity (GPP, $\mu mol\ m^{-2}s^{-1}$) under water-well conditions (DOY 110-117).

https://doi.org/10.5194/egusphere-2024-2940
Preprint. Discussion started: 15 October 2024

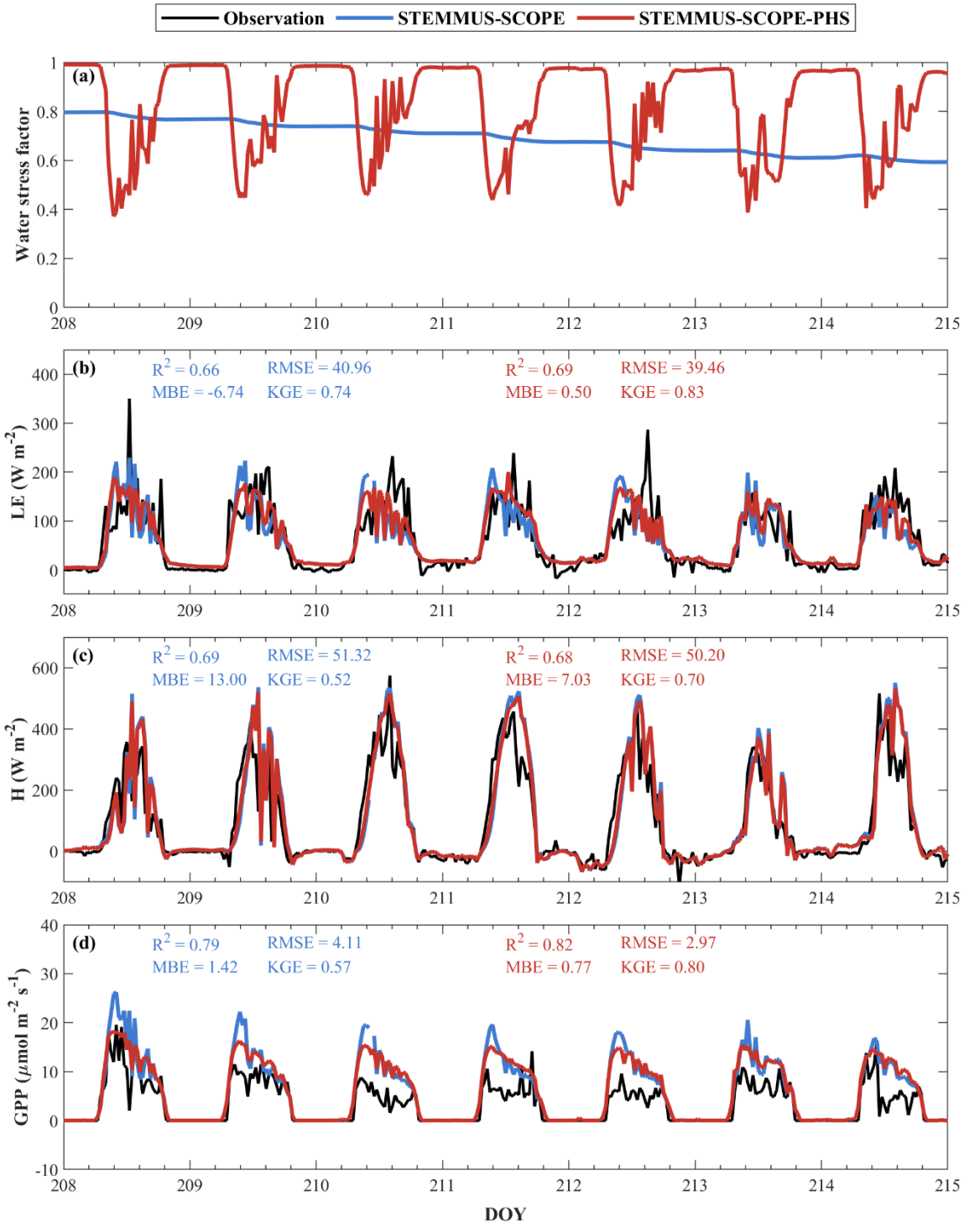

Figure 6: Diurnal dynamics for (a) water stress factor, (b) latent heat flux (LE, W m^{-2}), (c) sensible heat flux (H, W m^{-2}), and (d) gross primary productivity (GPP, $\mu mol\ m^{-2}s^{-1}$) under water-limited conditions (DOY 208-215).

https://doi.org/10.5194/egusphere-2024-2940
Preprint. Discussion started: 15 October 2024

3.3 Water potential gradients

In STEMMUS-SCOPE-PHS, the water fluxes in the plant vessel systems are described according to Darcy's law. The root, stem, and leaf water potentials are calculated. The comparison of simulated root zone soil, plant, and air-water potentials and the observed stem water potential are shown in Fig. 7. The range of root zone soil water potential is shown as the orange-shadow area in Fig. 7(a). The average root zone soil water potential is shown as the orange line. A slightly decreasing trend in root zone soil water potential and plant water potential (root, stem, and leaf) during this period is because the soil moisture decreases continuously via soil evaporation, root water uptake, and percolation. In addition, the averaged root zone soil water potential dominates the dynamics of root, stem and leaf water potential because it controls the water supply to the plant.

Compared with the root zone soil water potential (Fig. 7(b)), the plant water potential shows clear diurnal dynamics which results from the diurnal change of transpiration. In the nighttime, the value of plant water potential is close to the value of root zone soil water potential as roots absorb water from the soil until they equilibrium is reached. In the daytime, with the increase in air temperature and radiation, stomata open to capture carbon dioxide for photosynthesis. Inevitably, leaves release water via stomata to lower leaves' temperature which drops the leaf water potential to about -2 MPa till noon. The leaf water potential generally rises to the level of root zone soil water potential from noon to dawn on the next day. The simulated plant water potentials capture the trend of diurnal dynamics of root, stem and leaf water potential although the STEMMUS-SCOPE-PHS overestimates the stem water potential compared with observation. The reasons will be discussed in Section 4.

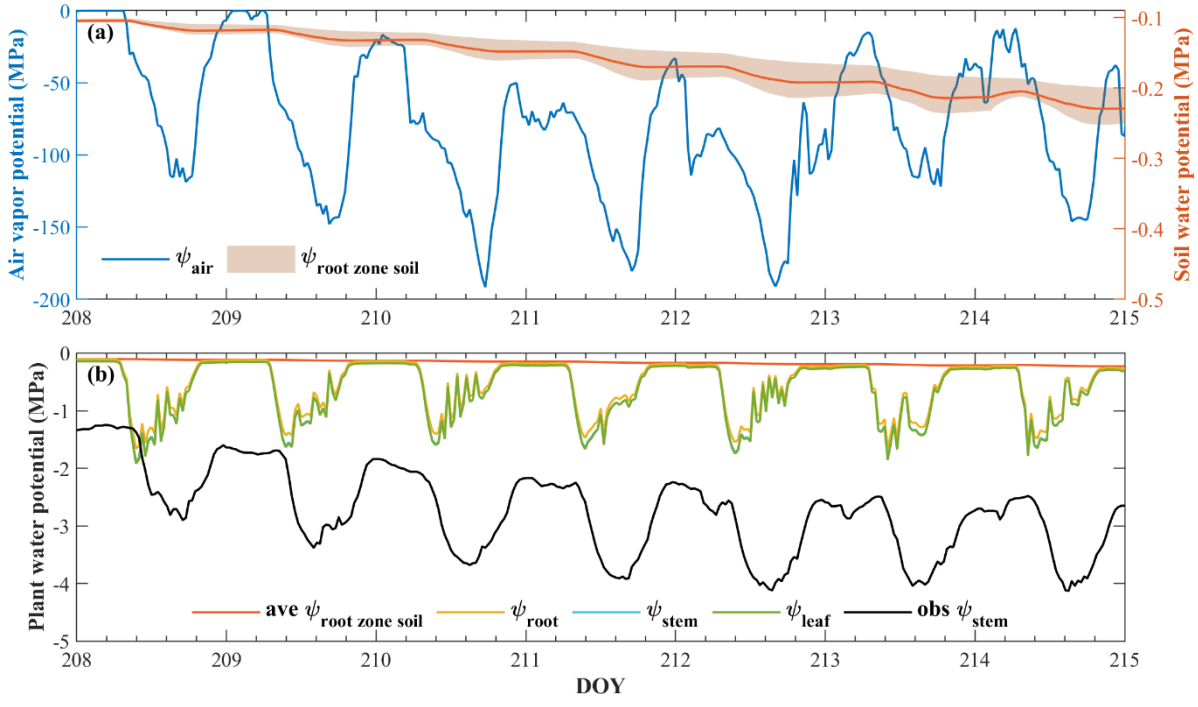

Figure 7: Comparison of simulated root zone soil ($\psi_{root\ zone\ soil}$), root (ψ_{root}), stem (ψ_{stem}), leaf (ψ_{leaf}) and air (ψ_{air}) water potential with observed stem water potential ($obs\ \psi_{stem}$).

https://doi.org/10.5194/egusphere-2024-2940
Preprint. Discussion started: 15 October 2024

4 Discussions

4.1 Influence of measured and calibrated G on energy fluxes validation

As shown in Fig. 3(d & h), the STEMMUS-SCOPE and STEMMUS-SCOPE-PHS show similar performance on simulations of G, indicating that the plant hydraulics process has limited impacts on G. It is important to note that the simulated half-hourly G represents the dynamics of G at the soil surface (0 cm). However, it is challenging to directly measure the G at the soil surface and avoid the influence of soil-atmosphere interaction, simultaneously (Gao et al., 2017). The in-situ measurement buries soil heat flux plates into the soil to reduce the influence from the land surface and obtains a reasonable baseline of G. Therefore, it's necessary to calibrate the observation from a specific depth (5 cm in this study) of the soil layer to surface layer. In the field observation, the thermal properties of soil heat flux plates are assumed to be equal to the thermal properties of soil to minimize the impacts of the plates on energy transfer in deeper soil layers. However, since the soil is heterogeneous, the thermal conductivity of the plate is not exactly the same as the thermal conductivity of the soil, which is the dominant source of measurement uncertainties (Gao et al., 2017). Secondly, the depth of the soil heat flux plate may change due to factors such as ground subsidence, precipitation and rills. It impacts the accuracy of observed soil heat flux. To make the observed G and simulated G comparable, the observed G is calibrated to the soil surface with the calorimetric method (Liebethal et al., 2005; Gao et al., 2017). The storage energy in the soil layer above the soil heat plate was calculated based on temperature gradient, and volumetric heat capacity. In this study, the radiation-retrieved land surface temperature is used as 0 cm soil temperature to calculate soil temperature gradient between 0 – 5 cm due to the lack of measurement on soil surface temperature. However, the land surface temperature represents a mixed soil-vegetation surface temperature rather than a bare soil temperature. This assumption may introduce uncertainties in the accuracy of calibrated G.

4.2 Parameterization on solar-induced chlorophyll fluorescence simulation

The dynamics of half-hourly SIF are shown in Fig. 4 and Fig. 8. The results show that the STEMMUS-SCOPE and STEMMUS-SCOPE-PHS have similar performance in the simulation of SIF, and both of them remarkably overestimate observed SIF because they are using the same parameterization (Van Der Tol et al., 2014). In STEMMUS-SCOPE, the emitted fluorescence (F) can be calculated as $F = \Phi_F \times PAR \times fPAR$, where Φ_F is quantum yield of fluorescence, and $fPAR$ is a fraction of absorbed PAR (Lee et al., 2015; Gu et al., 2019). The simulated and observed PAR are compared, and the results indicate that the simulated PAR agrees well with the observations either in water-well conditions or in water-limited conditions (Fig. 4 and Fig. 9). Therefore, the overestimation of SIF could be attributed to the simulation of fPAR and Φ_F. The dynamics of fPAR are highly related to canopy structure, and the chlorophyll content-related parameters. However, the canopy structure is assumed to be homogeneous and averagely divided into 30 layers in STEMMUS-SCOPE. The simplified canopy structure might contribute to the uncertainties in the radiative transfer process and introduce uncertainties in the simulation of fPAR. Besides, the chlorophyll-related parameters are set as constants based on plant function types for the whole study period. The inter-annual dynamics are ignored which might be a source of uncertainties in SIF simulation as well. The results highlight the

https://doi.org/10.5194/egusphere-2024-2940
Preprint. Discussion started: 15 October 2024

importance of considering heterogeneous canopy structure and seasonal chlorophyll parameters in understanding SIF dynamics.

Additionally, the parameterization of Φ_F in STEMMUS-SCOPE-PHS is based on an empirical electron transfer module (Van Der Tol et al., 2014) in which the rate efficiency of fluorescence, photochemistry, heat dissipation and non-photochemical quenching are empirical parameters, and the electron transport rate is determined by the CO_2 assimilation based on Farquhar-van Caemmerer-Berry model (Farquhar et al., 1980), which assumes the electron transport is not limited neither under water stress or nutrient stress. In the near future, the mechanistic process of the electron transport process (Gu et al., 2019; Han et al., 2022; Gu et al., 2023) and nutrient stress (Zhou et al., 2020; Cai et al., 2016; Fatichi et al., 2012) will be integrated into the STEMMUS-SCOPE-PHS model to improve our understanding on the relationship between photosynthesis and fluorescence.

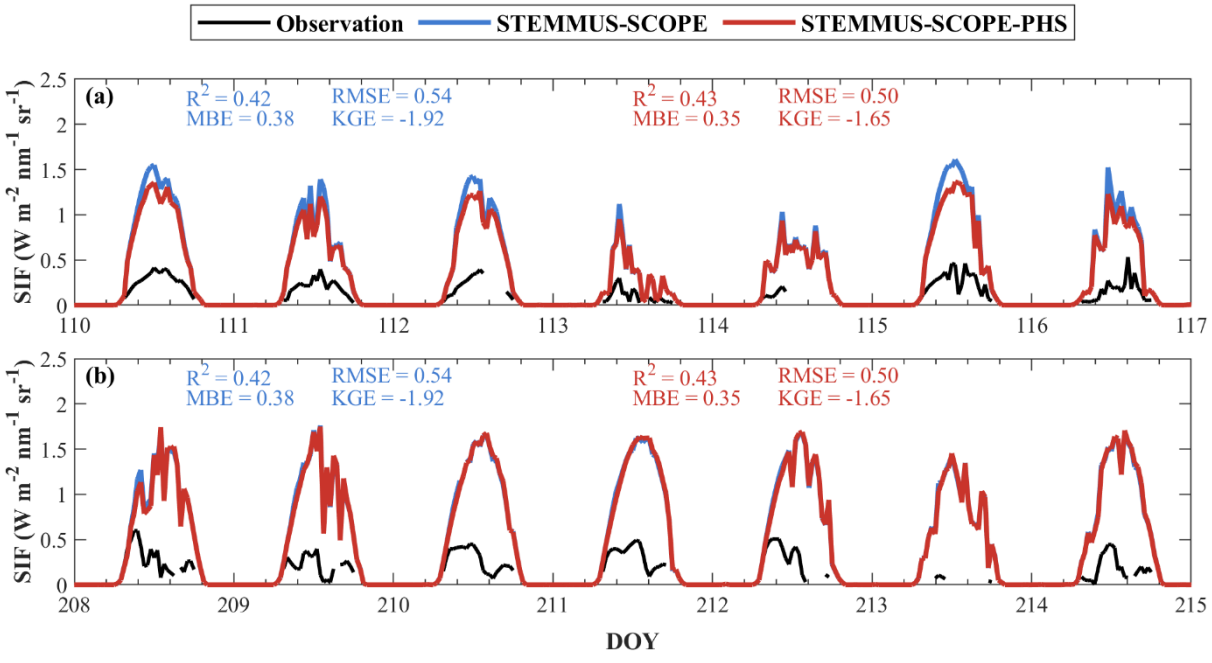

Figure 8: Comparison of half-hourly simulated and observed SIF at 760 nm. The black line is observed SIF. The blue and red line are simulated SIF by STEMMUS-SCOPE and STEMUS-SCOPE-PHS, respectively. (a) is water-well condition, and (b) is water-limited condition.

https://doi.org/10.5194/egusphere-2024-2940
Preprint. Discussion started: 15 October 2024

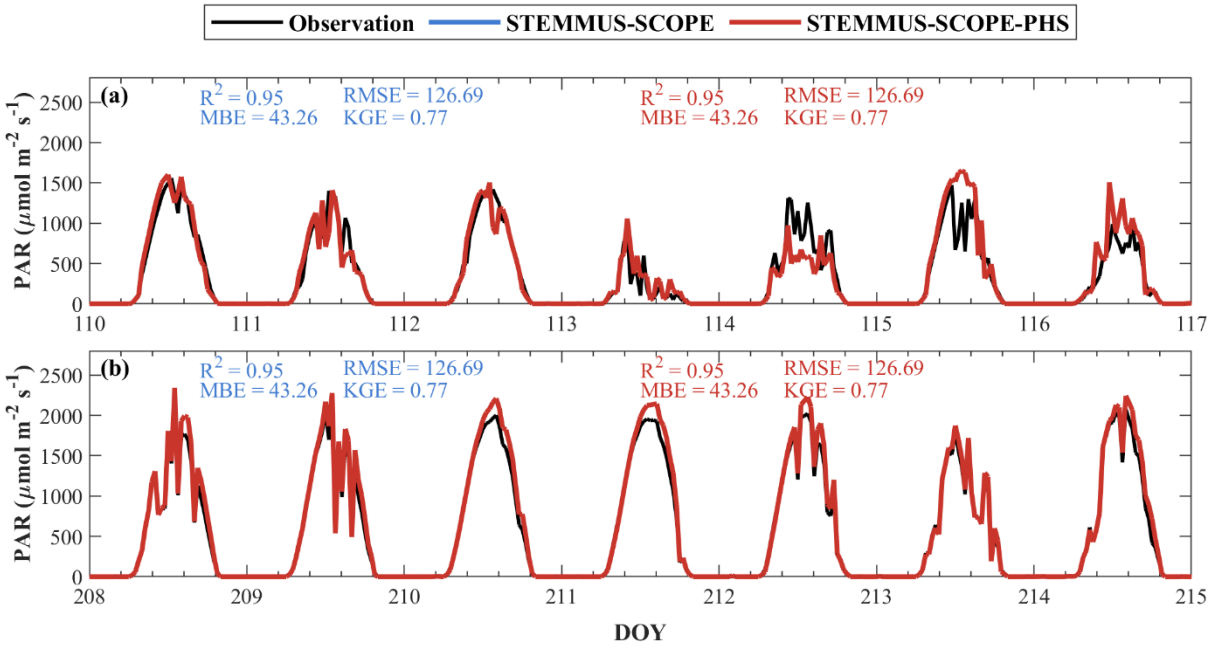

Figure 9: Comparison of half-hourly simulated and observed PAR. The black line is observed PAR, and the blue and red line are simulated PAR by STEMMUS-SCOPE and STEMUS-SCOPE-PHS, respectively, for which the blue and red lines overlap. (a) is water-well condition, and (b) is water-limited condition.

4.3 Comparison of water potentials

The simulated and observed plant water potentials were compared only on the water-limited condition (Fig. 7) due to the data availability of observed stem water potential. The trend of time-series plant water potentials is regulated by soil water potential (Carminati and Javaux, 2020). The ranges of plant water potentials are enveloped by the soil water potential and air vapor pressure since water always moves from high water potential to low water potential. As shown in Fig. 7(b), the model captured the diurnal dynamics of plant water potentials, but it overestimates the stem water potential compared with observation. One possible explanation is that stem and canopy water storage are not considered in STEMMUS-SCOPE-PHS. The ignorance of plant water storage may overestimate the water supply from roots and results in a less negative plant water potential compared with observation. This result suggests that plant water storage needs to be considered in further development.

5 Conclusion

A plant hydraulics module is implemented in STEMMUS-SCOPE-PHS to investigate the response of plants to water stress in a karst region in southwest China. In-situ data was collected from January to August 2022 over an evergreen broadleaf forest and was used to evaluate the model performance. Both STEMMUS-SCOPE and STEMMUS-SCOPE-PHS capture the temporal dynamics of the energy and carbon fluxes at the site scale. STEMMUS-SCOPE is found to overestimate the gross primary production (GPP) in the midday. In contrast, STEMMUS-SCOPE-PHS mitigates the discrepancy of the model

https://doi.org/10.5194/egusphere-2024-2940
Preprint. Discussion started: 15 October 2024

simulation by STEMMUS-SCOPE compared to the in-situ observation, decreasing the RMSE of GPP from 4.11 to 2.97 $\mu mol\ m^{-2}s^{-1}$ and increased KGE from 0.57 to 0.80. In addition, STEMMUS-SCOPE-PHS captures the diurnal dynamics of the water stress. However, both STEMMUS-SCOPE and STEMMUS-SCOPE-PHS overestimate the solar-induced chlorophyll fluorescence (SIF), as the electron transport limitation is not considered in the current version of the model, which is our ongoing research direction.

Appendix A

A1 Stomatal conductance scheme

In the STEMMUS-SCOPE model, the BallBerry's stomatal conductance scheme (Ball et al., 1987) was used as follow:

$$g_s = g_0 + m \cdot \frac{RH \cdot A_n}{c_a}, \quad (A1)$$

A2 Plant water stress factor and photosynthesis

The photosynthesis process can be described as follows in STEMMUS-SCOPE-PHS:

For C3 plants, water stress was used to constrain Vcmax in STEMMUS-SCOPE v1.0.0 (Wang et al., 2021);

$$V_c = V_{cmax} \cdot f_w, \quad (A2)$$

Plant water stress factor ($phwsf$) replaced soil water stress factor (f_w) in STEMMUS-SCOPE-PHS, and was calculated by leaf water potential

$$V_c = V_{cmax} \cdot phwsf, \quad (A3)$$

A3 Plant hydraulic pathway

A3.1 Root water uptake

A3.1.1 Root distribution

The distance between roots is calculated as:

$$dx_i = \sqrt{\frac{1}{\pi \times \rho_{rl}}}, \quad (A4)$$

where dx_i is the distance between roots (m), ρ_{rl} is root length per cubic meter (m m^{-3}).

A3.1.2 Root fractions

Root factions rf_i in soil layers are calculated as

https://doi.org/10.5194/egusphere-2024-2940
Preprint. Discussion started: 15 October 2024

$$rf_i = \begin{cases} (1-\beta^{0.5\cdot z_i}) & (i=1) \\ (\beta^{z_{i-1}-0.5\cdot\Delta z_{i-1}}) - \beta^{z_{i-1}+0.5\cdot\Delta z_i} & (i>1) \end{cases}, \quad (A5)$$

where β is a plant function type-dependent root distribution parameter (Jackson et al., 1997), z_i is the soil depth of the ith soil layer (m), Δz_i is the soil thickness of ith soil layer (m).

A3.1.3 Root length density

The root length density is calculated as (Wang et al., 2021)

$$\rho_{rl} = \frac{RTB}{B2C \cdot \rho_{root} \cdot \pi \cdot r_{root}^2} \cdot rf_i \cdot \frac{1}{\Delta z_i}, \quad (A6)$$

Where RTB is root to biomass, $B2C$ is the ratio to transfer biomass to carbon (0.488 gC gDM^{-1}), ρ_{root} is root density (gDM m^{-3}).r_{root} is root radius (1.5e-3 m).

A3.1.4 Root area index

The root area index (RAI, m^2 m^{-2}) is calculated as (Li et al., 2021)

$$RAI = (SAI + LAI) \cdot rf_i \cdot f_{root}, \quad (A7)$$

where SAI is stem area index (m^2 m^{-2}), LAI is leaf area index (m^2 m^{-2}), f_{root} is the allocation fraction of carbon assimilation to root (Wang et al., 2021). The SAI is set as a fraction of LAI:

$$SAI = s2l * LAI, \quad (A8)$$

where $s2l$ is the fraction of SAI to LAI.

A3.1.5 Soil conductance

The soil conductance $k_{s,i}$ (s^{-1}) is calculated as:

$$k_{s,i} = \frac{K_{soil,i}}{dx_i}, \quad (A9)$$

where $K_{soil,i}$ is unsaturated soil hydraulic conductivity (m s^{-1}), it is calculated as (Zeng and Su):

$$K_{soil,i} = K_{sat,i} \cdot {S_{e,i}}^{l} \cdot \left(1 - \left(1 - S_{e,i}^{\frac{1}{m}}\right)^m\right)^2, \quad (A10)$$

where $K_{sat,i}$ (m s^{-1}) is the saturated hydraulic conductivity, $S_{e,i}$ (unitless) is effective saturation, l and m are empirical parameters.

$$S_{e,i} = \frac{\theta_i - \theta_{res,i}}{\theta_{sat,i} - \theta_{res,i}}, \quad (A11)$$

where θ_i is soil moisture at the ith layer. $\theta_{res,i}$ and $\theta_{sat,i}$ are residual soil moisture and saturated soil moisture at the ith layer, respectively.

https://doi.org/10.5194/egusphere-2024-2940
Preprint. Discussion started: 15 October 2024

A3.1.6 Root vulnerability factor

The root vulnerability factor $phwsf_{root,i}$ is calculated as:

$$phwsf_{root,i} = \left[1 + \left(\frac{\psi_{soil,i}}{P50_{root}}\right)^{a_{root}}\right]^{-1}, \quad (A12)$$

where $\psi_{soil,i}$ (m) is soil water potential, $P50_{root}$ (m) is root water potential at the 50% hydraulic conductance loss. a_{root} is a shape factor.

A3.1.7 Root hydraulic conductance

The root hydraulic conductance $k_{root,i}$ (s^{-1}) is calculated as:

$$k_{root,i} = \frac{Kroot_{max}}{L+z_i} \cdot RAI \cdot phwsf_{root,i}, \quad (A13)$$

where $Kroot_{max}$ (m s^{-1}) is maximum root hydraulic conductivity, L (m) is root lateral length.

A3.1.8 Soil to root hydraulic conductance

The soil to root hydraulic conductance $k_{soil-root,i}$ (s^{-1}) is calculated as

$$k_{soil-root,i} = \frac{1}{\frac{1}{k_{s,i}} + \frac{1}{k_{root,i}}}, \quad (A14)$$

A3.2 Water flux from root to stem

A3.2.1 Stem vulnerability factor

The stem vulnerability factor $phwsf_{stem}$ is calculated as

$$phwsf_{stem} = \left[1 + \left(\frac{\psi_{root}}{P50_{stem}}\right)^{a_{stem}}\right]^{-1}, \quad (A15)$$

where ψ_{root} (m) is root water potential. $P50_{stem}$ (m) is stem water potential at 50% of hydraulic conductance loss. a_{stem} is a shape factor.

A3.2.2 Root to stem hydraulic conductance

The root to stem hydraulic conductance $k_{root-stem}$ (s^{-1}) is calculated as

$$k_{root-stem} = \frac{Kstem_{max}}{h} \cdot phwsf_{stem}, \quad (A16)$$

where $Kstem_{max}$ is stem hydraulic conductivity (m s^{-1}), h (m) is canopy height.

https://doi.org/10.5194/egusphere-2024-2940
Preprint. Discussion started: 15 October 2024

A3.3 Water flux from stem to leaf

A3.3.1 Leaf vulnerability factor

$$phwsf_{leaf} = \left[1 + \left(\frac{\psi_{stem}}{P50_{leaf}}\right)^{a_{leaf}}\right]^{-1}, \quad (A17)$$

where ψ_{stem} (m) is stem water potential. $P50_{leaf}$ (m) is leaf water potential at 50% of hydraulic conductance loss. a_{leaf} is a shape factor.

A3.3.2 Stem to leaf hydraulic conductance

$$k_{stem-leaf} = Kleaf_{max} \cdot phwsf_{leaf}, \quad (A18)$$

where $Kleaf_{max}$ (s^{-1}) is maximum leaf hydraulic conductance.

Code and data availability: The model development and data analysis are conducted via Matlab 2021a. The code of STEMMUS-SCOPE-PHS model can be downloaded at https://github.com/Crystal-szj/STEMMUS_SCOPE_ZSo_t1. The in-situ observation of meteorological and eddy covariance data was provided by Chongqing Jinfo Mountain Field Scientific Observation and Research Station, Southwest University, China.

Author contributions: Z.Song, Z.Su, Y.Zeng and M.Ma designed the study. Z.Song, X.Tang, Z.Zhu, Y.Xiao and D.Kong conducted field experiment and obtained in-situ observation data. Z.Song, Z.Su, Y.Zeng, Y.Wang, F. Alidoost and X.Han developed the code. Z.Song, Z.Su and Y.Zeng analyzed the data. Z.Song wrote the manuscript. Y.Zeng, Y.Wang, E.Tang, D.Yu and Z.Su revised the manuscript. All authors contributed to discussions throughout to develop this work.

Competing interests: At least one of the (co-)author is a member of the editorial board of Hydrology and Earth System Sciences.

Acknowledgement: This work was supported by the special fund for youth team of Southwest University (SWU-XJLJ202305), the Dutch Research Council (NWO) KIC, WUNDER project (grant no. KICH1.LWV02.20.004); the Netherlands eScience Center, EcoExtreML project (grant no. 27020G07), the National Natural Science Foundation of China (grant no. 42105119), and China Scholarship Council. We thank the technician Zhi Ding of Southwest University for providing AutoSIF observation data.

https://doi.org/10.5194/egusphere-2024-2940
Preprint. Discussion started: 15 October 2024

References

Abramowitz, G., Ukkola, A., Hobeichi, S., Cranko Page, J., Lipson, M., De Kauwe, M., Green, S., Brenner, C., Frame, J., Nearing, G., Clark, M., Best, M., Anthoni, P., Arduini, G., Boussetta, S., Caldararu, S., Cho, K., Cuntz, M., Fairbairn, D., Ferguson, C., Kim, H., Kim, Y., Knauer, J., Lawrence, D., Luo, X., Malyshev, S., Nitta, T., Ogee, J., Oleson, K., Ottlé, C., Peylin, P., de Rosnay, P., Rumbold, H., Su, B., Vuichard, N., Walker, A., Wang-Faivre, X., Wang, Y., and Zeng, Y.: On the predictability of turbulent fluxes from land: PLUMBER2 MIP experimental description and preliminary results, EGUsphere, 2024, 1-47, 10.5194/egusphere-2023-3084, 2024.

Adams, H. D., Zeppel, M. J. B., Anderegg, W. R. L., Hartmann, H., Landhäusser, S. M., Tissue, D. T., Huxman, T. E., Hudson, P. J., Franz, T. E., Allen, C. D., Anderegg, L. D. L., Barron-Gafford, G. A., Beerling, D. J., Breshears, D. D., Brodribb, T. J., Bugmann, H., Cobb, R. C., Collins, A. D., Dickman, L. T., Duan, H., Ewers, B. E., Galiano, L., Galvez, D. A., Garcia-Forner, N., Gaylord, M. L., Germino, M. J., Gessler, A., Hacke, U. G., Hakamada, R., Hector, A., Jenkins, M. W., Kane, J. M., Kolb, T. E., Law, D. J., Lewis, J. D., Limousin, J.-M., Love, D. M., Macalady, A. K., Martínez-Vilalta, J., Mencuccini, M., Mitchell, P. J., Muss, J. D., O'Brien, M. J., O'Grady, A. P., Pangle, R. E., Pinkard, E. A., Piper, F. I., Plaut, J. A., Pockman, W. T., Quirk, J., Reinhardt, K., Ripullone, F., Ryan, M. G., Sala, A., Sevanto, S., Sperry, J. S., Vargas, R., Vennetier, M., Way, D. A., Xu, C., Yepez, E. A., and McDowell, N. G.: A multi-species synthesis of physiological mechanisms in drought-induced tree mortality, Nature Ecology & Evolution, 1, 1285-1291, 10.1038/s41559-017-0248-x, 2017.

Anderegg, W. R. L., Klein, T., Bartlett, M., Sack, L., Pellegrini, A. F. A., Choat, B., and Jansen, S.: Meta-analysis reveals that hydraulic traits explain cross-species patterns of drought-induced tree mortality across the globe, Proceedings of the National Academy of Sciences, 113, 5024-5029, doi:10.1073/pnas.1525678113, 2016.

Anderegg, W. R. L., Flint, A., Huang, C.-y., Flint, L., Berry, J. A., Davis, Frank W., Sperry, J. S., and Field, C. B.: Tree mortality predicted from drought-induced vascular damage, Nature Geoscience, 8, 367-371, 10.1038/ngeo2400, 2015.

Anderegg, W. R. L., Konings, A. G., Trugman, A. T., Yu, K., Bowling, D. R., Gabbitas, R., Karp, D. S., Pacala, S., Sperry, J. S., Sulman, B. N., and Zenes, N.: Hydraulic diversity of forests regulates ecosystem resilience during drought, Nature, 561, 538-541, 10.1038/s41586-018-0539-7, 2018.

Ball, J. T., Woodrow, I. E., and Berry, J. A.: A Model Predicting Stomatal Conductance and its Contribution to the Control of Photosynthesis under Different Environmental Conditions, Biggins J. (eds) Progress in Photosynthesis Research, Springer, Dordrecht, https://doi.org/10.1007/978-94-017-0519-6_48, 1987.

Cai, X., Yang, Z. L., Fisher, J. B., Zhang, X., Barlage, M., and Chen, F.: Integration of nitrogen dynamics into the Noah-MP land surface model v1.1 for climate and environmental predictions, Geosci. Model Dev., 9, 1-15, 10.5194/gmd-9-1-2016, 2016.

Carminati, A. and Javaux, M.: Soil Rather Than Xylem Vulnerability Controls Stomatal Response to Drought, Trends in Plant Science, 25, 868-880, https://doi.org/10.1016/j.tplants.2020.04.003, 2020.

Choat, B., Brodribb, T. J., Brodersen, C. R., Duursma, R. A., López, R., and Medlyn, B. E.: Triggers of tree mortality under drought, Nature, 558, 531-539, 10.1038/s41586-018-0240-x, 2018.

Farquhar, G. D., von Caemmerer, S., and Berry, J. A.: A biochemical model of photosynthetic CO2 assimilation in leaves of C3 species, Planta, 149, 78-90, 10.1007/BF00386231, 1980.

Fatichi, S., Ivanov, V. Y., and Caporali, E.: A mechanistic ecohydrological model to investigate complex interactions in cold and warm water-controlled environments: 1. Theoretical framework and plot-scale analysis, Journal of Advances in Modeling Earth Systems, 4, https://doi.org/10.1029/2011MS000086, 2012.

Gao, Z., Russell, E. S., Missik, J. E. C., Huang, M., Chen, X., Strickland, C. E., Clayton, R., Arntzen, E., Ma, Y., and Liu, H.: A novel approach to evaluate soil heat flux calculation: An analytical review of nine methods, Journal of Geophysical Research: Atmospheres, 122, 6934-6949, https://doi.org/10.1002/2017JD027160, 2017.

Gatti, L. V., Basso, L. S., Miller, J. B., Gloor, M., Gatti Domingues, L., Cassol, H. L. G., Tejada, G., Aragão, L. E. O. C., Nobre, C., Peters, W., Marani, L., Arai, E., Sanches, A. H., Corrêa, S. M., Anderson, L., Von Randow, C., Correia, C. S. C., Crispim,

https://doi.org/10.5194/egusphere-2024-2940
Preprint. Discussion started: 15 October 2024

S. P., and Neves, R. A. L.: Amazonia as a carbon source linked to deforestation and climate change, Nature, 595, 388-393, 10.1038/s41586-021-03629-6, 2021.

Gu, L., Han, J., Wood, J. D., Chang, C. Y.-Y., and Sun, Y.: Sun-induced Chl fluorescence and its importance for biophysical modeling of photosynthesis based on light reactions, New Phytologist, 223, 1179-1191, https://doi.org/10.1111/nph.15796, 2019.

Gu, L., Grodzinski, B., Han, J., Marie, T., Zhang, Y.-J., Song, Y. C., and Sun, Y.: An exploratory steady-state redox model of photosynthetic linear electron transport for use in complete modelling of photosynthesis for broad applications, Plant, Cell & Environment, 46, 1540-1561, https://doi.org/10.1111/pce.14563, 2023.

Han, J., Chang, C. Y.-Y., Gu, L., Zhang, Y., Meeker, E. W., Magney, T. S., Walker, A. P., Wen, J., Kira, O., McNaull, S., and Sun, Y.: The physiological basis for estimating photosynthesis from Chla fluorescence, New Phytologist, 234, 1206-1219, https://doi.org/10.1111/nph.18045, 2022.

Jackson, R. B., Mooney, H. A., and Schulze, E.-D.: A global budget for fine root biomass, surface area, and nutrient contents, Proceedings of the National Academy of Sciences, 94, 7362-7366, doi:10.1073/pnas.94.14.7362, 1997.

Kennedy, D., Swenson, S., Oleson, K. W., Lawrence, D. M., Fisher, R., Lola da Costa, A. C., and Gentine, P.: Implementing Plant Hydraulics in the Community Land Model, Version 5, Journal of Advances in Modeling Earth Systems, 11, 485-513, https://doi.org/10.1029/2018MS001500, 2019.

Konings, A. G. and Gentine, P.: Global variations in ecosystem-scale isohydricity, Global Change Biology, 23, 891-905, https://doi.org/10.1111/gcb.13389, 2017.

Lawrence, D. M., Fisher, R. A., Koven, C. D., Oleson, K. W., Swenson, S. C., Bonan, G., Collier, N., Ghimire, B., van Kampenhout, L., Kennedy, D., Kluzek, E., Lawrence, P. J., Li, F., Li, H., Lombardozzi, D., Riley, W. J., Sacks, W. J., Shi, M., Vertenstein, M., Wieder, W. R., Xu, C., Ali, A. A., Badger, A. M., Bisht, G., van den Broeke, M., Brunke, M. A., Burns, S. P., Buzan, J., Clark, M., Craig, A., Dahlin, K., Drewniak, B., Fisher, J. B., Flanner, M., Fox, A. M., Gentine, P., Hoffman, F., Keppel-Aleks, G., Knox, R., Kumar, S., Lenaerts, J., Leung, L. R., Lipscomb, W. H., Lu, Y., Pandey, A., Pelletier, J. D., Perket, J., Randerson, J. T., Ricciuto, D. M., Sanderson, B. M., Slater, A., Subin, Z. M., Tang, J., Thomas, R. Q., Val Martin, M., and Zeng, X.: The Community Land Model Version 5: Description of New Features, Benchmarking, and Impact of Forcing Uncertainty, Journal of Advances in Modeling Earth Systems, 11, 4245-4287, https://doi.org/10.1029/2018MS001583, 2019.

Lee, J.-E., Berry, J. A., van der Tol, C., Yang, X., Guanter, L., Damm, A., Baker, I., and Frankenberg, C.: Simulations of chlorophyll fluorescence incorporated into the Community Land Model version 4, Global Change Biology, 21, 3469-3477, https://doi.org/10.1111/gcb.12948, 2015.

Li, L., Yang, Z. L., Matheny, A. M., Zheng, H., Swenson, S. C., Lawrence, D. M., Barlage, M., Yan, B., McDowell, N. G., and Leung, L. R.: Representation of Plant Hydraulics in the Noah-MP Land Surface Model: Model Development and Multiscale Evaluation, Journal of Advances in Modeling Earth Systems, 13, e2020MS002214, 10.1029/2020ms002214, 2021.

Liebethal, C., Huwe, B., and Foken, T.: Sensitivity analysis for two ground heat flux calculation approaches, Agricultural and Forest Meteorology, 132, 253-262, https://doi.org/10.1016/j.agrformet.2005.08.001, 2005.

Limousin, J. M., Rambal, S., Ourcival, J. M., Rocheteau, A., Joffre, R., and Rodriguez-Cortina, R.: Long-term transpiration change with rainfall decline in a Mediterranean Quercus ilex forest, Global Change Biology, 15, 2163-2175, 10.1111/j.1365-2486.2009.01852.x, 2009.

Mackay, D. S., Roberts, D. E., Ewers, B. E., Sperry, J. S., McDowell, N. G., and Pockman, W. T.: Interdependence of chronic hydraulic dysfunction and canopy processes can improve integrated models of tree response to drought, Water Resources Research, 51, 6156-6176, https://doi.org/10.1002/2015WR017244, 2015.

McDowell, N. G., Brodribb, T. J., and Nardini, A.: Hydraulics in the 21st century, New Phytologist, 224, 537-542, https://doi.org/10.1111/nph.16151, 2019.

Medlyn, B. E., Duursma, R. A., Eamus, D., Ellsworth, D. S., Prentice, I. C., Barton, C. V. M., Crous, K. Y., De Angelis, P.,

https://doi.org/10.5194/egusphere-2024-2940
Preprint. Discussion started: 15 October 2024

Freeman, M., and Wingate, L.: Reconciling the optimal and empirical approaches to modelling stomatal conductance, Global Change Biology, 17, 2134-2144, 10.1111/j.1365-2486.2010.02375.x, 2011.

Powell, T. L., Galbraith, D. R., Christoffersen, B. O., Harper, A., Imbuzeiro, H. M. A., Rowland, L., Almeida, S., Brando, P. M., da Costa, A. C. L., Costa, M. H., Levine, N. M., Malhi, Y., Saleska, S. R., Sotta, E., Williams, M., Meir, P., and Moorcroft, P. R.: Confronting model predictions of carbon fluxes with measurements of Amazon forests subjected to experimental drought, New Phytologist, 200, 350-365, https://doi.org/10.1111/nph.12390, 2013.

Song, L., Li, Y., Ren, Y., Wu, X., Guo, B., Tang, X., Shi, W., Ma, M., Han, X., and Zhao, L.: Divergent vegetation responses to extreme spring and summer droughts in Southwestern China, Agricultural and Forest Meteorology, 279, 107703, https://doi.org/10.1016/j.agrformet.2019.107703, 2019.

Tang, E., Zeng, Y., Wang, Y., Song, Z., Yu, D., Wu, H., Qiao, C., van der Tol, C., Du, L., and Su, Z.: Understanding the effects of revegetated shrubs on fluxes of energy, water, and gross primary productivity in a desert steppe ecosystem using the STEMMUS–SCOPE model, Biogeosciences, 21, 893-909, 10.5194/bg-21-893-2024, 2024.

Torres-Ruiz, J. M., Cochard, H., Delzon, S., Boivin, T., Burlett, R., Cailleret, M., Corso, D., Delmas, C. E. L., De Caceres, M., Diaz-Espejo, A., Fernández-Conradi, P., Guillemot, J., Lamarque, L. J., Limousin, J.-M., Mantova, M., Mencuccini, M., Morin, X., Pimont, F., De Dios, V. R., Ruffault, J., Trueba, S., and Martin-StPaul, N. K.: Plant hydraulics at the heart of plant, crops and ecosystem functions in the face of climate change, New Phytologist, 241, 984-999, https://doi.org/10.1111/nph.19463, 2024.

Tuzet, A., Perrier, A., and Leuning, R.: A coupled model of stomatal conductance, photosynthesis and transpiration, Plant, Cell & Environment, 26, 1097-1116, https://doi.org/10.1046/j.1365-3040.2003.01035.x, 2003.

TYREE, M. T. and EWERS, F. W.: The hydraulic architecture of trees and other woody plants, New Phytologist, 119, 345-360, https://doi.org/10.1111/j.1469-8137.1991.tb00035.x, 1991.

van der Tol, C., Berry, J. A., Campbell, P. K., and Rascher, U.: Models of fluorescence and photosynthesis for interpreting measurements of solar-induced chlorophyll fluorescence, J Geophys Res Biogeosci, 119, 2312-2327, 10.1002/2014JG002713, 2014.

van der Tol, C., Verhoef, W., Timmermans, J., Verhoef, A., and Su, Z.: An integrated model of soil-canopy spectral radiances, photosynthesis, fluorescence, temperature and energy balance, Biogeosciences, 6, 3109-3129, 10.5194/bg-6-3109-2009, 2009.

Wang, Y., Sun, Y., Chen, Y., Wu, C., Huang, C., Li, C., and Tang, X.: Non-linear correlations exist between solar-induced chlorophyll fluorescence and canopy photosynthesis in a subtropical evergreen forest in Southwest China, Ecological Indicators, 157, 111311, https://doi.org/10.1016/j.ecolind.2023.111311, 2023.

Wang, Y., Zeng, Y., Song, Z., Yu, D., Han, Q., Tang, E., de Bruin, H., and Su, Z.: On the Estimation of Global Plant Water Requirement, EGUsphere, 2024, 1-18, 10.5194/egusphere-2024-1321, 2024.

Wang, Y., Zeng, Y., Yu, L., Yang, P., Van der Tol, C., Yu, Q., Lü, X., Cai, H., and Su, Z.: Integrated modeling of canopy photosynthesis, fluorescence, and the transfer of energy, mass, and momentum in the soil–plant–atmosphere continuum (STEMMUS–SCOPE v1.0.0), Geoscientific Model Development, 14, 1379-1407, 10.5194/gmd-14-1379-2021, 2021.

Wutzler, T., Lucas-Moffat, A., Migliavacca, M., Knauer, J., Sickel, K., Šigut, L., Menzer, O., and Reichstein, M.: Basic and extensible post-processing of eddy covariance flux data with REddyProc, Biogeosciences, 15, 5015-5030, 10.5194/bg-15-5015-2018, 2018.

Xiao, Y., Zhao, W., Ma, M., and He, K.: Gap-Free LST Generation for MODIS/Terra LST Product Using a Random Forest-Based Reconstruction Method, Remote Sensing, 13, 2828, 2021.

Xie, S., Mo, X., Liu, S., and Hu, S.: Plant hydraulics improves predictions of ET and GPP responses to drought, Water Resources Research, n/a, e2022WR033402, https://doi.org/10.1029/2022WR033402, 2023.

Xu, X., Medvigy, D., Powers, J. S., Becknell, J. M., and Guan, K.: Diversity in plant hydraulic traits explains seasonal and inter-annual variations of vegetation dynamics in seasonally dry tropical forests, New Phytol, 212, 80-95, 10.1111/nph.14009,

https://doi.org/10.5194/egusphere-2024-2940
Preprint. Discussion started: 15 October 2024

2016.

Zeng, Y. and Su, B.: STEMMUS introduction manual,

Zeng, Y. and Su, Z.: Digital twin approach for the soil-plant-atmosphere continuum: think big, model small, Frontiers in Science, 2, 10.3389/fsci.2024.1376950, 2024.

Zeng, Y., Su, Z., Wan, L., and Wen, J.: A simulation analysis of the advective effect on evaporation using a two-phase heat and mass flow model, Water Resources Research, 47, https://doi.org/10.1029/2011WR010701, 2011a.

Zeng, Y., Su, Z., Wan, L., and Wen, J.: Numerical analysis of air-water-heat flow in unsaturated soil: Is it necessary to consider airflow in land surface models?, Journal of Geophysical Research: Atmospheres, 116, https://doi.org/10.1029/2011JD015835, 2011b.

Zhou, X. R., Schnepf, A., Vanderborght, J., Leitner, D., Lacointe, A., Vereecken, H., and Lobet, G.: CPlantBox, a whole-plant modelling framework for the simulation of water- and carbon-related processes, In Silico Plants, 2, 10.1093/insilicoplants/diaa001, 2020.